Analysis of the classical phase space and energy transfer for two rotating dipoles with and without external electric field

Rosario González-Férez,[1] Manuel Iñarrea,[2] J. Pablo Salas,[2] and Peter Schmelcher[3,4]

[1]*Instituto Carlos I de Física Teórica y Computacional, and Departamento de Física Atómica, Molecular y Nuclear,
Universidad de Granada, 18071 Granada, Spain*
[2]*Área de Física, Universidad de La Rioja, 26006 Logroño, La Rioja, Spain*
[3]*The Hamburg Center for Ultrafast Imaging, Luruper Chaussee 149, 22761 Hamburg, Germany*
[4]*Zentrum für Optische Quantentechnologien, Universität Hamburg, Luruper Chaussee 149, 22761 Hamburg, Germany*

We explore the classical dynamics of two interacting rotating dipoles that are fixed in the space and exposed to an external homogeneous electric field. Kinetic energy transfer mechanisms between the dipoles are investigated by varying both the amount of initial excess kinetic energy of one of them and the strength of the electric field. In the field-free case, and depending on the initial excess energy, an abrupt transition between equipartition and nonequipartition regimes is encountered. The study of the phase space structure of the system as well as the formulation of the Hamiltonian in an appropriate coordinate frame provide a thorough understanding of this sharp transition. When the electric field is turned on, the kinetic energy transfer mechanism is significantly more complex and the system goes through different regimes of equipartition and nonequipartition of the energy including chaotic behavior.

I. INTRODUCTION

The mechanism of energy exchange between molecules, mediated either by the Coulomb, dipole-dipole, or van der Waals interactions, is an active research area with several intriguing perspectives in physics, chemistry, biology, and materials sciences. The wide range of applications covers, for instance, the photosynthesis of plants and bacteria [1–5], the emission of light of organic materials [6–8], and molecular crystals [9–11]. On the other hand, cooling and trapping cold molecules in an optical lattice allow one to fix their positions while exploiting their interactions [12,13]. The latter becomes particularly interesting for strongly polar diatomic systems where the dipole-dipole interaction is sufficiently long range that novel structural as well as dynamical and collective behaviors can be expected [14–16]. External electric fields provide then a versatile tool to control these interactions, e.g., the alignment of the dipoles with the field [17].

One of the most popular approaches to investigate the energy transfer in a many-body system is to describe it by a linear chain of nonlinear oscillators with different coupling between them. These models are based on the seminal work of Fermi, Pasta, and Ulam [18], the so-called FPU system. This work was the first to realize that, in the infinite time limit, this system of nonlinear oscillators does not reach the expected smooth energy-equipartition behavior. After several decades of research and a plethora of works, see, for instance, Refs. [19–25], the question concerning the energy sharing mechanism in a chain of nonlinear oscillators, and, therefore, in a many-body system can be considered still an open question. Furthermore, in Refs. [26–28] the energy flow in a linear chain of interacting rotating dipoles and in a two-dipole system are explored. For the two-dipole system, the authors conclude the existence of a critical excitation energy up to which there is no energy transfer.

In order to provide further insights in the energy transfer mechanisms in dipole chains, in this work, we consider two interacting rotating dipoles exposed to an external electric field. One important motivation to select this model is to mimic the dipole-dipole interaction between two cold polar diatomic molecules trapped in an optical lattice. The aim is to investigate the classical phase space in relation to the energy transfer mechanism between the two rotors, both in the absence and in the presence of an electric field. Assuming that their positions are fixed in space, we employ a classical description of their internal dynamics within the rigid rotor approximation. A certain amount of kinetic energy is then given to one of the dipoles and the energy transfer mechanism between the two dipoles is explored as the excess kinetic energy and the field strength are varied. For the field-free system, we encounter energy-equipartition and nonequipartition regimes depending on the initial excess energy. In the field-dressed system, there exists a competition between the anisotropic dipole-dipole interaction of the rotors and the electric field interaction. If the strengths of these two interactions are comparable, the classical dynamics is chaotic. As the strength of the electric field increases, and the field interaction dominates, we encounter an energy-equipartition regime that is followed by an energy-localized one for even stronger fields.

The paper is organized as follows: In Sec. II we establish the classical rotational Hamiltonian governing the dynamics of two identical rotating dipoles in an external electric field with fixed spatial positions. The equations of motion and the critical points in an invariant manifold are also presented. Sections III and IV are devoted to the investigation of the exchange of energy between the two rotors in the field-free case and in the presence of the external field, respectively. The conclusions are provided in Sec. V.

II. CLASSICAL HAMILTONIAN AND EQUATIONS OF MOTION

We consider two identical dipoles, fixed in space and separated by a distance a_l along the laboratory fixed frame

(LFF) X axis. Here, we employ the rigid rotor approximation to describe the dynamics of the two dipoles. In the presence of an external homogeneous time-dependent electric field parallel to the LFF Z axis and with strength $\mathcal{E}_s(t)$, the interaction potential, $\mathcal{V} \equiv \mathcal{V}(\theta_1, \phi_1, \theta_2, \phi_2, t)$, can be shown to be as follows [26,28,29]:

$$\mathcal{V} = -\mu \mathcal{E}_s(t)(\cos\theta_1 + \cos\theta_2) + \frac{\mu^2}{4\pi\epsilon_0 a_l^3}[\cos\theta_1 \cos\theta_2$$
$$+ \sin\theta_1 \sin\theta_2(\sin\phi_1 \sin\phi_2 - 2\cos\phi_1 \cos\phi_2)], \quad (1)$$

where (θ_i, ϕ_i), with $i = 1, 2$, represent the Euler angles of each rotor. The first term in (1) stands for the interaction of the dipole moment, μ, of the two rotors with the external electric field of strength $\mathcal{E}_s(t) = E_s f(t)$ that is turned on with the linear function

$$f(t) = \begin{cases} \frac{t}{t_1} & \text{if} \quad 0 \leqslant t < t_1, \\ 1 & \text{if} \quad t \geqslant t_1. \end{cases} \quad (2)$$

This linear ramp-up envelope was previously used in Ref. [30] and it mimics more complex theoretical [31] and experimental laser pulses [32]. The last term in (1) represents the dipole-dipole interaction between the two rotors. The classical Hamiltonian describing the rotational motion of this system reads

$$\mathcal{H} = \sum_{i=1}^{2} \frac{1}{2I}\left[P_{\theta_i}^2 + \frac{P_{\phi_i}^2}{\sin^2\theta_i}\right] + \mathcal{V}, \quad (3)$$

where I is the moment of inertia of the dipoles, and where the first two terms stand for the rotational kinetic energy of the dipoles. Expression (3) defines a $(4 + 1/2)$-degree-of-freedom Hamiltonian dynamical system in $(\theta_1, \phi_1, \theta_2, \phi_2)$, in the corresponding momenta $(P_{\theta_1}, P_{\phi_1}, P_{\theta_2}, P_{\phi_2})$ and in time. For the sake of simplicity, it is convenient to handle a dimensionless Hamiltonian. Since our model is relevant to describing two interacting rigid-rotor polar diatomic molecules, it is natural to express energy in units of the molecular rotational constant $B = \hbar^2/2I$ and time in units of the characteristic time $t_B = \hbar/2B$. In this way, we arrive at the dimensionless Hamiltonian given by

$$H \equiv \frac{\mathcal{H}}{B} = \sum_{i=1}^{2}\left[P_{\theta_i}^2 + \frac{P_{\phi_i}^2}{\sin^2\theta_i}\right] + V, \quad (4)$$

with the rescaled potential, $V \equiv V(\theta_1, \phi_1, \theta_2, \phi_2, t)$, being

$$V = -f(t)\beta(\cos\theta_1 + \cos\theta_2) + \chi[\cos\theta_1 \cos\theta_2$$
$$+ \sin\theta_1 \sin\theta_2(\sin\phi_1 \sin\phi_2 - 2\cos\phi_1 \cos\phi_2)], \quad (5)$$

where the dimensionless parameters

$$\chi = \frac{\mu^2}{4\pi\epsilon_0 a_l^3 B} \quad \text{and} \quad \beta = \frac{\mu E_s}{B} \quad (6)$$

control the dipole-dipole and electric field interactions, respectively.

Since the two rotors are identical, Hamiltonian (4) possesses an exchange symmetry of even character. Moreover, Hamiltonian (4) presents two invariant manifolds,

namely,

$$\mathcal{M} = \{(\theta_1, \theta_2, P_{\theta_1}, P_{\theta_2}) \mid \phi_1 = \phi_2 = P_{\phi_1} = P_{\phi_2} = 0\}, \quad (7)$$
$$\mathcal{N} = \{(\theta_1, \theta_2, P_{\theta_1}, P_{\theta_2}) \mid \phi_1 = \phi_2 = \pi/2, P_{\phi_1} = P_{\phi_2} = 0\}, \quad (8)$$

where the dynamics is limited to planar motions confined to the XZ plane and to the YZ plane, respectively. Our study focuses on the invariant manifold $\mathcal{M}$ because for $\beta = 0$, the field-free case, the Hamiltonian associated to Eq. (7) is structurally stable in the sense that, if we slightly perturb this model away from the manifold $\mathcal{M}$, the dynamics remains in the neighborhood of $\phi_1 = \phi_2 = P_{\phi_1} = P_{\phi_2} = 0$. However, for $\beta = 0$, the Hamiltonian system described by Eq. (8) is structurally unstable because trajectories starting in the vicinity of $\phi_1 = \phi_2 = \pi/2$, $P_{\phi_1} = P_{\phi_2} = 0$ tend to move away from the manifold $\mathcal{N}$. This instability is due to the fact that the Hessian matrix associated to $\mathcal{N}$ is singular for $\beta = 0$. As a consequence of this singular character of the Hessian matrix, the potential energy surface associated to $\mathcal{N}$ has no critical points for $\beta = 0$.

In the invariant manifold $\mathcal{M}$, the Hamiltonian reads

$$H_{\mathcal{M}} \equiv \mathcal{E} = P_1^2 + P_2^2 + V_{\mathcal{M}}(\theta_1, \theta_2, t), \quad (9)$$

where $V_{\mathcal{M}}(\theta_1, \theta_2, t) \equiv V(\theta_1, 0, \theta_2, 0, t)$ is the potential energy surface of this system in $\mathcal{M}$. In the rest of the paper, we focus our study on the manifold $\mathcal{M}$. The Hamiltonian equations of motion arising from $H_{\mathcal{M}}$ read as follows:

$$\dot{\theta}_1 = 2P_1, \quad \dot{\theta}_2 = 2P_2,$$
$$\dot{P}_1 = [\chi \cos\theta_2 - \beta f(t)]\sin\theta_1 + 2\chi \cos\theta_1 \sin\theta_2,$$
$$\dot{P}_2 = [\chi \cos\theta_1 - \beta f(t)]\sin\theta_2 + 2\chi \cos\theta_2 \sin\theta_1. \quad (10)$$

A. The critical points of the energy surface

Part of the dynamics can be inferred from the landscape of the potential energy surface $V_{\mathcal{M}}(\theta_1, \theta_2, t)$, and its critical points, which are the equilibrium points of the Hamiltonian flux (10) equated to zero. Since Hamiltonian (9) is an even function with exchange symmetry, the critical points are located along the directions $\theta_1 = \theta_2$ and $\theta_1 = -\theta_2$. Note that, for the sake of completeness, the polar angles (θ_1, θ_2) are varied in the interval $(-\pi, \pi)$. For $t \geqslant t_1$ $[f(t) = 1]$ the electric field parameter has reached it maximal value β and the critical points of $V_{\mathcal{M}}(\theta_1, \theta_2, t)$ are the roots of the equations

$$(\beta - 3\chi \cos\theta_1)\sin\theta_1 = 0 \quad \text{with} \quad \theta_2 = \theta_1,$$
$$(\beta + \chi \cos\theta_1)\sin\theta_1 = 0 \quad \text{with} \quad \theta_2 = -\theta_1. \quad (11)$$

There exist five critical points, their conditions of existence and stability and energies are summarized in Table I. The positions and energies of these critical points as the electric field parameter β increases are presented in Fig. 1.

For $0 \leqslant \beta/\chi < 1$, the five equilibria exist. In the field-free case $\beta = 0$, the energy surface $V_{\mathcal{M}}(\theta_1, \theta_2, t \geqslant t_1)$ shows the characteristic landscape of the dipole-dipole interaction shown in Fig. 2(a). The minima $\mathcal{C}_1$ correspond to the stable *head-tail* configurations of the dipoles, while the maxima $\mathcal{C}_5$ correspond to the unstable *head-head* or *tail-tail* configurations. Thus,

TABLE I. Conditions of existence, stability, and energy of the critical points of $V_{\mathcal{M}}(\theta_1,\theta_2,t > t_1)$. The saddle points are denoted by SP.

Equilibrium	Existence	Stability	Energy $\mathcal{E}$
$C_1 = (\pm\cos^{-1}(\beta/3\chi),\pm\cos^{-1}(\beta/3\chi))$	$\beta \leqslant 3\chi$	Minima	$\mathcal{E}_1 = -(6\chi^2 + \beta^2)/3\chi$
$C_2 = (\pm\pi,0),\ (0,\pm\pi)$	Always	SP	$\mathcal{E}_2 = -\chi$
$C_3 = (0,0)$	Always	If $\beta < 3\chi$, SP; if $\beta > 3\chi$, minimum	$\mathcal{E}_3 = \chi - 2\beta$
$C_4 = (\pm\pi,\pm\pi) \equiv (\pm\pi,\mp\pi)$	Always	If $\beta < \chi$, SP; if $\beta > \chi$, maxima	$\mathcal{E}_4 = \chi + 2\beta$
$C_5 = (\pm\cos^{-1}(-\beta/\chi),\mp\cos^{-1}(-\beta/\chi))$	$\beta \leqslant \chi$	Maxima	$\mathcal{E}_5 = (2\chi^2 + \beta^2)/\chi$

if the energy of the system is below the energy of the saddle points C_2, $\mathcal{E}_2 = -\chi$, the two dipoles are confined in the potential wells created by the minima C_1 and they oscillate around the stable head-tail configuration. If the energy of the system is larger than $\mathcal{E}_2 = -\chi$, and smaller than the energy of the saddle points C_3 and C_4, $\mathcal{E}_3 = \mathcal{E}_4 = \chi$, the oscillations of the dipoles are of large amplitude but still around the stable head-tail configurations. Finally, if the total energy is larger than $\mathcal{E}_3 = \mathcal{E}_4 = \chi$, the rotors can perform complete rotations.

For $0 < \beta/\chi < 1$, as the ratio β/χ approaches 1, the minima C_1 (maxima C_5) move towards the saddle point C_3 (C_4). However, the shape of the energy surface $V_{\mathcal{M}}(\theta_1,\theta_2,t \geqslant t_1)$ remains qualitatively the same, though being somewhat distorted as compared to the field-free case; see Fig. 2(b) for $\beta/\chi = 0.9$. As a rough approximation, for $0 < \beta/\chi < 1$, the interaction due to the electric field could be considered a perturbation to the dipole-dipole interaction, which dominates the dynamics. For $\beta/\chi = 1$, a pitchfork bifurcation takes place between the saddle points C_4 and the maxima C_5 (see Fig. 1), and from there on only the saddle points C_4, which become maxima, survive, which is illustrated in Fig. 2(c) for $\beta/\chi = 1.1$. As the electric field parameter increases in the interval $1 \leqslant \beta/\chi < 3$, the minima C_1 keep moving towards C_3; see Fig. 1 and the contour plot in Fig. 2(d) for $\beta/\chi = 2.9$. At $\beta/\chi = 3$, C_1 and C_3 collide and a second pitchfork bifurcation occurs. From this bifurcation on, only the critical point C_3 survives now as minimum; see Fig. 2(e) for $\beta/\chi = 3.1$. For $\beta/\chi \geqslant 3$, the shape of the energy surface $V_{\mathcal{M}}(\theta_1,\theta_2,t = t_1)$ is qualitatively similar to the $\chi = 0$ case, where only the interaction due to the electric field is taken into account; cf. Figs. 2(e) and 2(f). Indeed, for $\beta/\chi \geqslant 3$, the dipole-dipole interaction could be considered a perturbation to the electric field interaction.

B. The rotated reference system

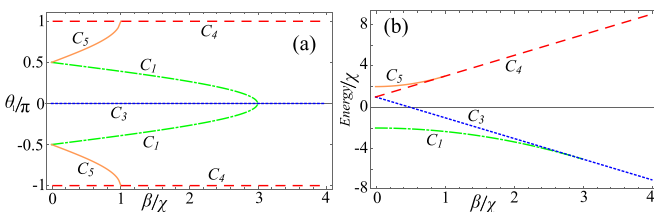A $3\pi/4$ rotation around the axis perpendicular to the plane (θ_1,θ_2) of Hamiltonian (9) takes the equilibria along the bisector $\theta_2 = \theta_1$ to the axis $\theta_2 = 0$. This rotation is a canonical transformation between the coordinates $(\theta_1,\theta_2,P_1,P_2)$ and the new ones $(\theta_1',\theta_2',P_1',P_2')$ given by

$$\theta_1' = \frac{\theta_1 + \theta_2}{\sqrt{2}}, \quad \theta_2' = \frac{\theta_2 - \theta_1}{\sqrt{2}},$$

$$P_1' = \frac{P_1 + P_2}{\sqrt{2}}, \quad P_2' = \frac{P_2 - P_1}{\sqrt{2}}, \tag{12}$$

and with generating function $\mathcal{W}$:

$$\mathcal{W} = P_1'\left(\frac{\theta_1 + \theta_2}{\sqrt{2}}\right) + P_2'\left(\frac{\theta_2 - \theta_1}{\sqrt{2}}\right). \tag{13}$$
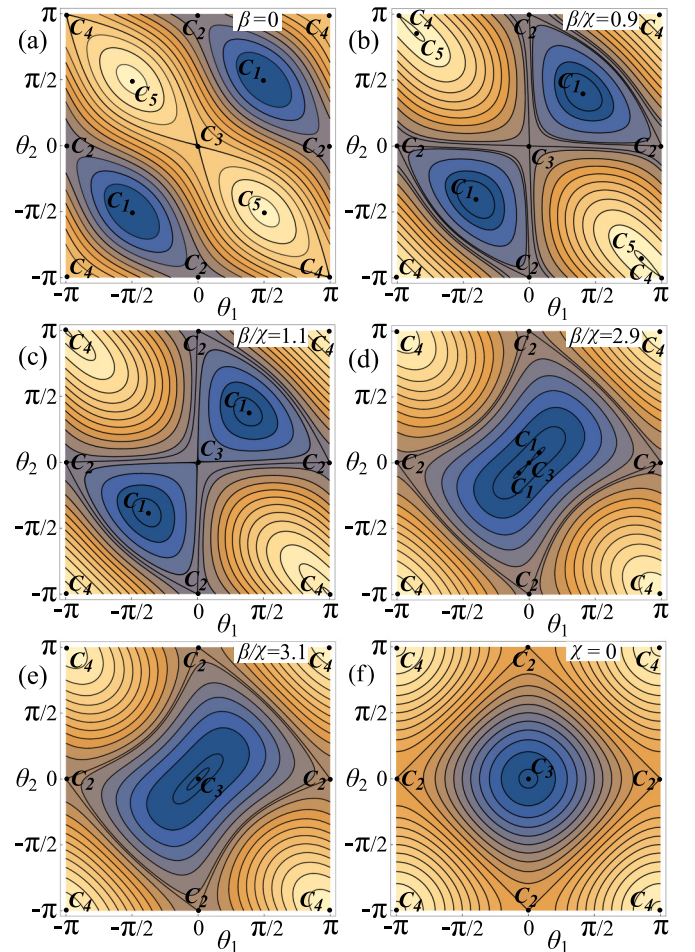

FIG. 1. Evolution of the (a) position and (b) energy of the critical points of $V_{\mathcal{M}}(\theta_1,\theta_2,t \geqslant t_1)$ as a function of the ratio between the electric field parameter β and the dipole-dipole interaction parameter χ.

FIG. 2. Evolution of the landscape of the potential energy surface $V_{\mathcal{M}}(\theta_1,\theta_2,t)$ for $t > t_1$ and different values of the ratio between electric field parameter and the dipole-dipole interaction β/χ.
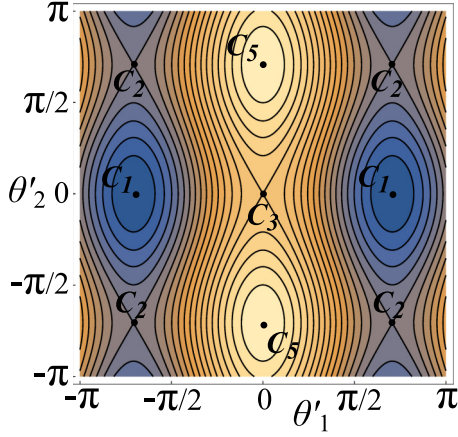
FIG. 3. Landscape of the rotated potential energy surface $V'(\theta_1', \theta_2', t)$ for $\beta = 0$. The period of the rotated potential for $\beta = 0$ is $\pi/\sqrt{2}$, but for the sake of clarity, we plot it in the interval $[-\pi, \pi]$.

The rotated Hamiltonian H' reads

$$H' = E' = P_1'^2 + P_2'^2 + V'_{\mathcal{M}}(\theta_1', \theta_2', t), \qquad (14)$$

where

$$V'_{\mathcal{M}}(\theta_1', \theta_2', t) = V_1'(\theta_1') + V_2'(\theta_2')$$
$$- 2\beta f(t) \cos\left(\frac{\theta_1'}{\sqrt{2}}\right) \cos\left(\frac{\theta_2'}{\sqrt{2}}\right), \quad (15)$$

with

$$V_1'(\theta_1') = \tfrac{3}{2}\chi \cos(\sqrt{2}\,\theta_1'), \quad V_2'(\theta_2') = -\tfrac{1}{2}\chi \cos(\sqrt{2}\,\theta_2').$$

The potential $V'_{\mathcal{M}}(\theta_1', \theta_2', t)$ represents the potential energy of two pendula coupled by the external electric field. Note that the period of these pendula is $\pi/\sqrt{2}$.

In the field-free case, $\beta = 0$, the dipole-dipole Hamiltonian is separable, $H' = H_1' + H_2'$, with

$$H_1' = E_1' = P_1'^2 + \tfrac{3}{2}\chi \cos(\sqrt{2}\,\theta_1'),$$
$$H_2' = E_2' = P_2'^2 - \tfrac{1}{2}\chi \cos(\sqrt{2}\,\theta_2'), \qquad (16)$$

and the dynamics is that of two uncoupled pendula. The contour plot of $V'_{\mathcal{M}}(\theta_1', \theta_2', t)$ for $\beta = 0$ is depicted in Fig. 3.

III. ENERGY TRANSFER IN THE FIELD-FREE CASE

In this section, we explore the energy transfer mechanism between the two field-free rotors assuming that, initially, they do not have the same kinetic energy. Indeed, we assume that initially the two rotors are at rest, with zero kinetic energy, in the bottom of the potential well $\mathcal{C}_1$, i.e., $\theta_1 = \theta_2 = \pi/2$, in the stable head-tail configuration with total energy -2χ. From this situation, we assume that a certain amount of kinetic energy $\delta\mathcal{K}$ is given to the first dipole, in such a way that the initial conditions at $t = 0$ are

$$\theta_1(0) = \theta_2(0) = \frac{\pi}{2}, \quad P_1(0) = \sqrt{\delta\mathcal{K}}, \quad P_2(0) = 0. \quad (17)$$

With these initial conditions, the Hamiltonian equations of motion (10) for $\beta = 0$ are integrated up to a final time t_f by means of an explicit eighth-order Runge-Kutta algorithm with
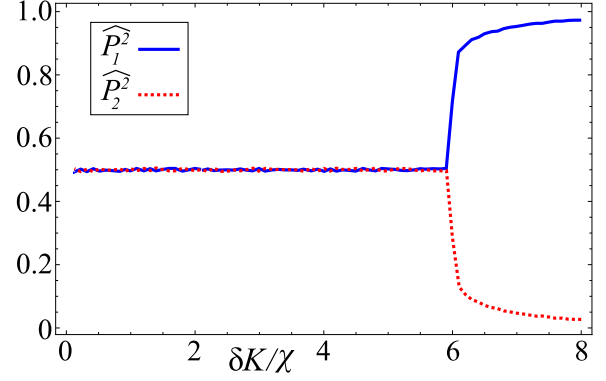

FIG. 4. For the field-free system, the normalized time-averaged kinetic energies of the dipoles $\widehat{P_1^2}$ (solid blue line) and $\widehat{P_2^2}$ (dotted red line), see (18), as a function of the initial excess energy of the first dipole $\delta\mathcal{K}$. The dipole-dipole interaction strength is $\chi = 1 \times 10^{-5}$.

step-size control and dense output [33]. During the numerical integration, we compute the normalized time average of the kinetic energy of each dipole, $\widehat{P_i^2}$, given by

$$\widehat{P_i^2} = \frac{\langle P_i^2 \rangle}{\langle P_1^2 \rangle + \langle P_2^2 \rangle}, \quad \langle P_i^2 \rangle = \frac{1}{t_f - t_1} \int_{t_1}^{t_f} P_i^2(t)\,dt. \quad (18)$$

Note that in the field-free case $\beta = 0$, and we use $t_1 = 0$. The outcome depends on the parameter of the dipole-dipole interaction χ and the amount of excess energy $\delta\mathcal{K}$. Here, we fix the dipole-dipole interaction and investigate the energy transfer as the energy given to the first dipole increases. This dipole-dipole interaction parameter depends on the molecular species, through the rotational constant and permanent electric dipole moment, and on the separation between the dipoles. In this work, we use $\chi = 1 \times 10^{-5}$. In case we were considering the dipoles to be cold LiCs molecules trapped in an optical lattice, the value $\chi = 1 \times 10^{-5}$ would correspond to an optical lattice with $a_l = 429$ nm. The parameter $\delta\mathcal{K}$ is given in units of χ, i.e., in the energy units of the potential energy surface $V_{\mathcal{M}}(\theta_1, \theta_2, t)$ for $\beta = 0$, and we investigate the interval $0\chi \leqslant \delta\mathcal{K} \leqslant 8\chi$. The final time is fixed to $t_f = 5 \times 10^4$. Our numerical tests have shown that this value for the stopping time is appropriate for the correct characterization of the outcomes.

The normalized time-averaged kinetic energies of the dipoles are shown in Fig. 4 as the excess energy $\delta\mathcal{K}$ increases. If the excess energy $\delta\mathcal{K}$ is smaller than the critical value $\delta\mathcal{K}_c \approx 6\chi$, the system is in an equipartition-energy regime, $\widehat{P_1^2}$ is very close to $\widehat{P_2^2}$, and there is a continuous energy flow between the rotors. This behavior is illustrated for $\delta\mathcal{K} = 4\chi$ in Fig. 5(a) with the time evolution of the kinetic energies $P_1^2(t)$ and $P_2^2(t)$, and the potential energy $V_{\mathcal{M}}(\theta_1, \theta_2, t)$. For $\delta\mathcal{K} \approx 6\chi$, this equipartition regime abruptly breaks and for $\delta\mathcal{K} \gtrsim 6\chi$, most of the kinetic energy remains in the first dipole. As a consequence, the energy flow between the dipoles is interrupted as shown in Fig. 5(b) for $\delta\mathcal{K} = 7\chi$. The dynamics of this first rotor is essentially different in these two regimes. For $\delta\mathcal{K} < 6\chi$, the kinetic energy $P_1^2(t)$ oscillates and reaches zero as a minimal value [see Fig. 5(a)], which indicates a noncontinuous rotation and this first dipole is at rest at these minima. For $\delta\mathcal{K} > 6\chi$, $P_1^2(t) > 0$, cf. Fig. 5(b), which
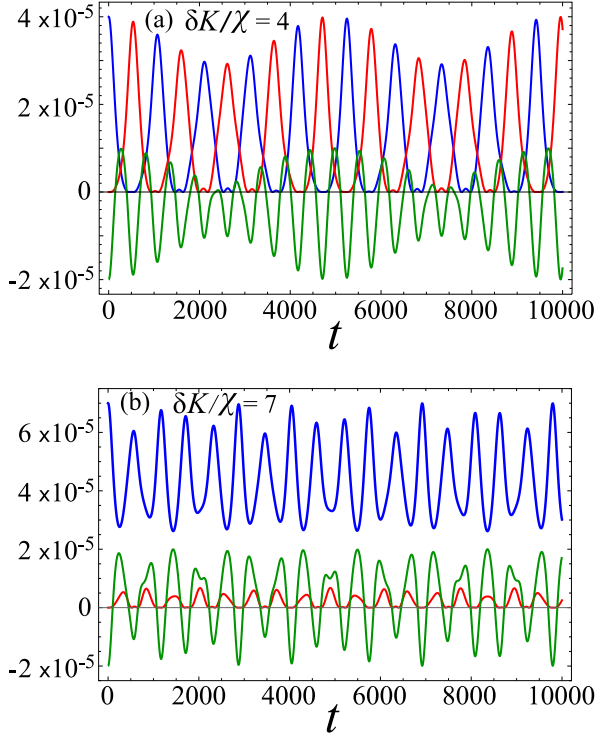
FIG. 5. For the field-free system, time evolution of the kinetic energies $P_1^2(t)$ (blue lines) and $P_2^2(t)$ (red lines) and the potential energy $V_{\mathcal{M}}(\theta_1,\theta_2,t)$ (green lines). The initial excess energies of the first dipole are (a) $\delta\mathcal{K} = 4\chi$ and (b) $\delta\mathcal{K} = 7\chi$. The dipole-dipole interaction strength is $\chi = 1 \times 10^{-5}$.

indicates that the first dipole is performing a continuous rotation. In contrast, the smaller kinetic energy of the second rotor $P_2^2(t)$ oscillates with a noncontinuous rotation and has as a minimum value zero in both regimes. This behavior in the energy flux between the dipoles was already observed by de Jonge *et al.* [28]. In that paper, the authors provide an analytical explanation showing that the energy transfer is only possible in a low energy regime.

To gain a deeper physical insight into the energy transfer mechanism, we present in Fig. 6 the Poincaré surface of section in the plane (P_1,θ_1) with $\theta_2 = \pi/2$ for three initial excess energies. This surface of section provides a good illustration for the trajectory τ with initial conditions (17). For $\delta\mathcal{K}_c < 6\chi$,

the orbit τ has a vibrational nature [see Fig. 6(a)], whereas we observe in Fig. 6(c) that its nature becomes rotational for $\delta\mathcal{K}_c > 6\chi$. At the critical value $\delta\mathcal{K}_c = 6\chi$, the τ orbit is the separatrix [cf. Fig. 6(b)] that keeps rotational and vibrational regions away from each other. That is why the transition from the energy equipartition regime to the nonequipartition occurs at the critical value $\delta\mathcal{K}_c = 6\chi$.

These energy transfer mechanisms can be explained analyzing the dynamics of the two pendula in the rotated reference frame. The momenta in the LFF and in the rotated frame are related according to

$$P_1 = \frac{P_1' - P_2'}{\sqrt{2}}, \quad P_2 = \frac{P_1' + P_2'}{\sqrt{2}}, \tag{19}$$

and the time-averaged kinetic energy of each dipole can be written as

$$\langle P_1^2 \rangle = \frac{\langle P_1'^2 \rangle + \langle P_2'^2 \rangle}{2} - \langle P_1' P_2' \rangle, \tag{20}$$

$$\langle P_2^2 \rangle = \frac{\langle P_1'^2 \rangle + \langle P_2'^2 \rangle}{2} + \langle P_1' P_2' \rangle; \tag{21}$$

that is, the time-averaged kinetic energies of the dipoles differ by twice the time average of the product of momenta of the pendula, $\langle P_1' P_2' \rangle$.

In the rotated reference frame, using the transformations (12), the initial conditions $(\theta_1(0), P_1(0), \theta_2(0), P_2(0))$ give rise to two (uncoupled) pendular motions governed by Hamiltonians (16) with energies E_1' and E_2'. These energies determine the motion in the rotated frame and the kinetic energy transfer mechanism between the rotors. If the energies of the pendula are smaller than the maxima of the potentials $V_1'(\theta_1')$ and $V_2'(\theta_2')$, i.e., $E_1' < 3\chi/2$ and $E_2' < \chi/2$, respectively, the total energy of the system is $E = E_1' + E_2' < 2\chi$, and both pendula describe periodic oscillations, i.e., the momenta P_1' and P_2' are periodic functions around zero with $\langle P_1' \rangle = \langle P_2' \rangle = 0$, and the time-averaged product $\langle P_1' P_2' \rangle$ is zero. As a consequence, $\langle P_1^2 \rangle = \langle P_2^2 \rangle$, which means that the system will always belong to the equipartition kinetic energy regime. The same behavior occurs when $E_1' > 3\chi/2$ or $E_2' > \chi/2$, and at least one of them is in the vibrational regime with $\langle P_i' \rangle = 0$, whereas the other one describes complete periodic rotations and its momentum is a periodic function around a nonzero value having a nonzero time average, and again it holds that $\langle P_1' P_2' \rangle = 0$. Finally, if the initial condition
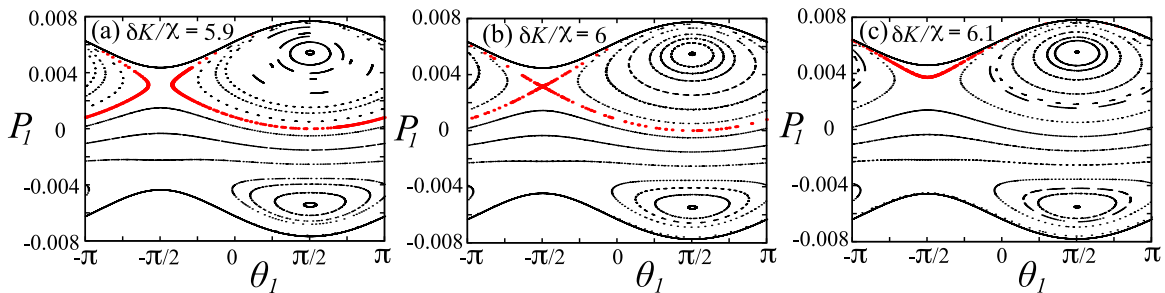

FIG. 6. For the field-free system with dipole-dipole interaction $\chi = 1 \times 10^{-5}$, Poincaré surfaces of section in the plane (P_1,θ_1) with $\theta_2 = \pi/2$ for three different initial excess energies in the neighborhood of the critical value $\delta\mathcal{K}_c = 6\chi$. The red thick points correspond to the trajectory τ with initial conditions (17).
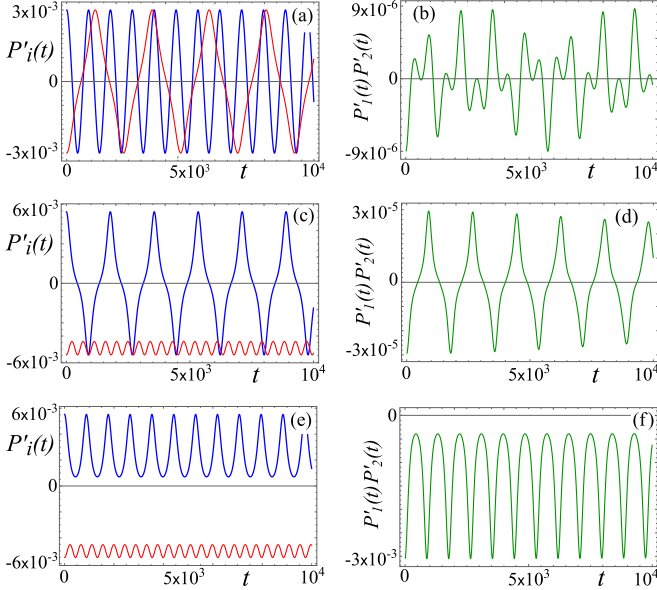
FIG. 7. For the field-free system, time evolution of the momenta $P'_1(t)$ (blue lines) and $P'_2(t)$ (red lines) of the uncoupled pendula (left column) and the product $P'_1(t)P'_2(t)$ (green lines, right column) for the excess energies (a, b) $\delta\mathcal{K} = 1.8\chi$, (c, d) $\delta\mathcal{K} = 5.9\chi$, and (e, f) $\delta\mathcal{K} = 6.1\chi$, for $P'_1(t)$ and $P'_2(t)$, and $P'_1(t)P'_2(t)$, respectively. The dipole-dipole interaction strength is $\chi = 1 \times 10^{-5}$.

FIG. 8. The normalized time-averaged kinetic energies of the dipoles $\widehat{P_1^2}$ (blue solid line) and $\widehat{P_2^2}$ (red dashed line) as a function of the ratio between the electric field parameter β and the dipole-dipole parameter χ for two initial excess energies of the first rotor (a,c) $\delta\mathcal{K} = 4\chi$ and (b,d) $\delta\mathcal{K} = 7\chi$. The dipole-dipole interaction parameter is set to $\chi = 1 \times 10^{-5}$. The ramp-up time for the electric field is $t_1 = 1200$ in panels (a) and (b) and $t_1 = 600$ in panels (c) and (d).

leads to a pendular energy distribution with $E'_1 > 3\chi/2$ and $E'_2 > \chi/2$, then both pendula are in the rotational regime, the time-averaged product $\langle P'_1 P'_2 \rangle$ is nonzero, and the equipartition regime is not met.

For the orbit τ, the initial conditions (17) expressed in the rotated frame read

$$\theta'_1(0) = \frac{\pi}{\sqrt{2}}, \quad \theta'_2(0) = 0, \quad P'_1(0) = \sqrt{\frac{\delta\mathcal{K}}{2}}, \quad P'_2(0) = -\sqrt{\frac{\delta\mathcal{K}}{2}}.$$

In this rotated frame, the excess kinetic energies in the pendula are the same, $\delta\mathcal{K}/2$, whereas their energies are

$$E'_1 = \frac{\delta\mathcal{K}}{2} - \frac{3}{2}\chi, \quad E'_2 = \frac{\delta\mathcal{K}}{2} - \frac{1}{2}\chi. \qquad (22)$$

If the excess energy satisfies $\delta\mathcal{K} < 2\chi$, both pendula are in an oscillatory motion, and the dipoles belong to the energy equipartition regime. This is illustrated for $\delta\mathcal{K} = 1.8\chi$ in Figs. 7(a) and 7(b) with the time evolution of $P'_1(t)$, $P'_2(t)$ and $P'_1(t)P'_2(t)$, respectively. If the excess energy satisfies $2\chi < \delta\mathcal{K} < 6\chi$, the second pendulum performs complete rotations, whereas the first one still performs a vibrational motion [see in Figs. 7(c) and 7(d) the evolution of the momenta and the product of momenta for $\delta\mathcal{K} = 5.9\chi$]. In this situation, the dipole relaxes again to the equipartition regime. However, if the excess energy is $\delta\mathcal{K} > 6\chi$, both pendula have a rotational motion and the dipoles do not reach the equipartition regime. As an example see for $\delta\mathcal{K} = 6.1\chi$ the time evolution of the momenta and the product of momenta in Figs. 7(e) and 7(f).
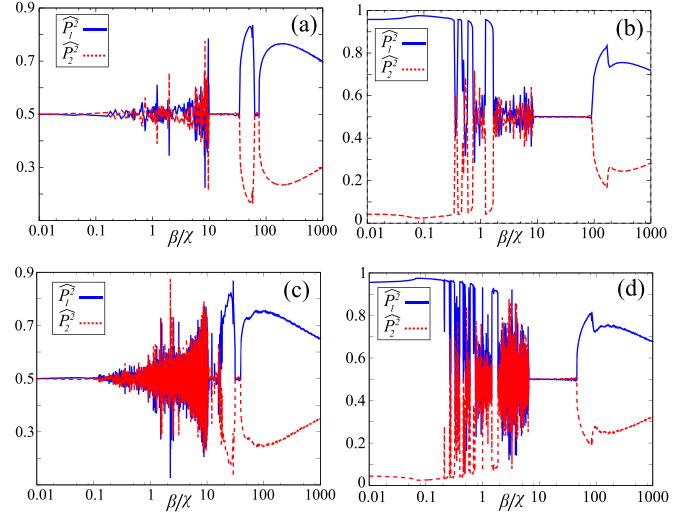
IV. ENERGY TRANSFER IN AN EXTERNAL ELECTRIC FIELD

In this section we explore the energy transfer between the two dipoles in the presence of an external electric field. Again, we assume that the dipoles are initially in the stable head-tail configuration with zero kinetic energy. At time $t = 0$, a certain amount of kinetic energy $\delta\mathcal{K}$ is given to the first dipole, and simultaneously the electric field is turned on with the linear profile (2). Using the initial conditions (17), the equations of motion (10) are integrated up to a final time t_f, and we compute the normalized time-averaged momenta $\widehat{P_1^2}$ and $\widehat{P_2^2}$ from (18). As in the field-free system, we are using a dipole-dipole interaction with strength $\chi = 1 \times 10^{-5}$, and a final time $t_f = 5 \times 10^4$. The strength of the electric field is varied in the interval $0.01\chi \leqslant \beta \leqslant 1000\chi$. Based on the results for the field-free system, we investigate the time-averaged kinetic energies $\widehat{P_1^2}$ and $\widehat{P_2^2}$ for $\delta\mathcal{K} = 4\chi$ and $\delta\mathcal{K} = 7\chi$ as the field parameter varies. In order to explore also the influence of the ramp-up of the field, we perform our calculations for $t_1 = 1200$ and $t_1 = 600$, which roughly correspond to 100 and 50 ns, respectively, which could be achieved in current experiments with realistic field strengths. The results are depicted in Fig. 8. For the two excess energies and for the longer ramp-up $t_1 = 1200$, $\widehat{P_1^2}$ and $\widehat{P_2^2}$ follow essentially different behaviors as β increases [see Figs. 8(a) and 8(b)]. However, four common patterns can be identified in Figs. 8(a) and 8(b). For small values $\beta \lesssim 0.2\chi$, the dipole-dipole interaction is dominant and adding the external electric field has no relevant effect. As a consequence, we encounter the energy partition regimes for $\delta\mathcal{K} = 4\chi$ (equipartition for $\beta = 0$) and $\delta\mathcal{K} = 7\chi$ (nonequipartition for $\beta = 0$). By increasing the electric field in the interval $0.5\chi \lesssim \beta \lesssim 20\chi$, the energy partition diagrams
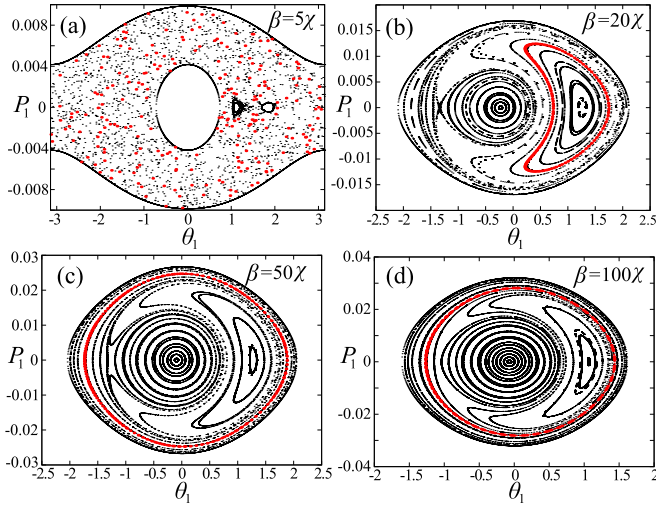
FIG. 9. Poincaré surface of section in the plane (P_1, θ_1) with $P_2 = 0$ for different values of the electric field parameter β. The dipole-dipole interaction is $\chi = 1 \times 10^{-5}$ and the excess kinetic energy of the first dipole is $\delta\mathcal{K} = 4\chi$. The thick (red) points correspond to the trajectory τ with initial conditions (17).

FIG. 10. The same as in Fig. 9, but for an excess energy of the first dipole of $\delta\mathcal{K} = 7\chi$.

show sudden (irregular) variations; see Figs. 8(a) and 8(b). In this field range, the dipole-dipole and the electric field interactions are comparable in magnitude and the system dynamics is very sensitive to the variations of the electric field parameter. For intermediate strengths, the dipoles relax to an energy equipartition regime: see Figs. 8(a) and 8(b) in the intervals $10\chi \lesssim \beta \lesssim 40\chi$ and $10\chi \lesssim \beta \lesssim 100\chi$, for $\delta\mathcal{K} = 4\chi$ and $\delta\mathcal{K} = 7\chi$, respectively. Finally, for stronger electric fields, the system falls out of the equipartition regime, and most of the kinetic energy remains in one of the dipoles. For the initial conditions investigated here, most of the kinetic energy remains in the first dipole. By varying the initial conditions, the role played by the two rotors could change, and the second rotor could store most of the kinetic energy. For the shorter ramp-up time $t_1 = 600$, we find a qualitatively similar behavior as for the $t_1 = 1200$ case [see Figs. 8(c) and 8(d)], but a higher global sensitivity. Due to this higher sensitivity, we observe larger irregular variations in the intermediate interval $0.1\chi \lesssim \beta \lesssim 10\chi$.

The Poincaré surfaces of section provide a global picture of the phase space structure and are therefore suited to analyze and understand the kinetic energy transfer. We analyze the Poincaré surfaces of section for a fixed $t > t_1$, once the electric field parameter has reached its maximal strength β and the energy is constant. To illustrate the trajectory τ with initial conditions (17), a suitable surface of section for the Poincaré map is given by the intersection of the phase space trajectories with the plane (P_1, θ_1) with $P_2 = 0$. In Figs. 9 and 10, we show these Poincaré surfaces of section for different values of the electric field parameter β and for the excess energies $\delta\mathcal{K} = 4\chi$ and $\delta\mathcal{K} = 7\chi$, respectively.

For $\beta = 5\chi$, the system shows a sensitive dependence on the electric field parameter (cf. Fig. 8), and the Poincaré surfaces of section exhibit a chaotic sea. A single trajectory with initial conditions in this sea covers randomly a large portion of the Poincaré map [see Figs. 9(a) and 10(a)].
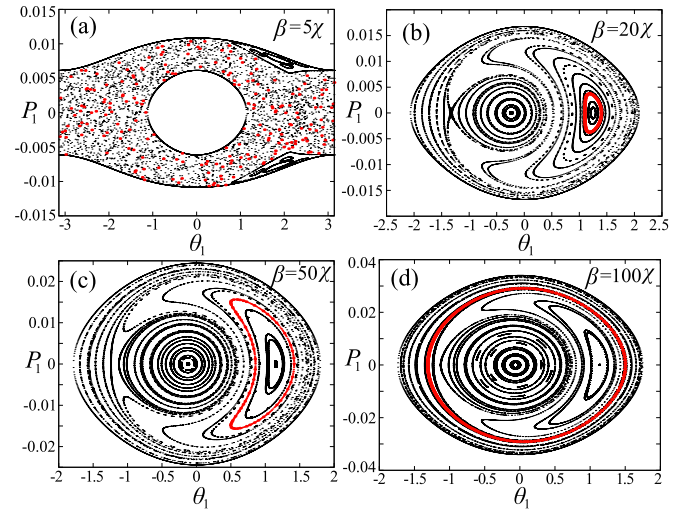
In particular, the chaotic sea of these surfaces of section results in strongly fluctuating kinetic energies $P_1^2(t)$ and $P_2^2(t)$, as shown in Fig. 11(a) for the orbit τ with $\delta\mathcal{K} = 4\chi$ and $\beta = 5\chi$. For stronger electric fields, the phase space of the system is made up of three different types of regular Kolmogorov-Arnold-Moser (KAM) tori organized around two stable periodic orbits and kept apart by a separatrix attached to an unstable periodic orbit (see Figs. 9 and 10). Each type of KAM torus corresponds to one of the kinetic energy partition regimes detected in Fig. 8. Indeed, when the dipoles are in the energy equipartition regime, the trajectory τ falls inside the KAM torus centered around the stable periodic orbit located on the right-hand side of the Poincaré surfaces of section. This is observed for the surfaces of section for $\beta = 20\chi$ with $\delta\mathcal{K} = 4\chi$ and $\delta\mathcal{K} = 7\chi$ in Figs. 9(b) and 10(b), respectively, and $\beta = 50\chi$ and $\delta\mathcal{K} = 7\chi$ in Fig. 10(c). The equipartition energy is manifest in the time evolution of the kinetic energies $P_1^2(t)$ and $P_2^2(t)$ presented in Fig. 11(b) for $\delta\mathcal{K} = 20\chi$ and $\beta = 20\chi$. In contrast, if the system falls out
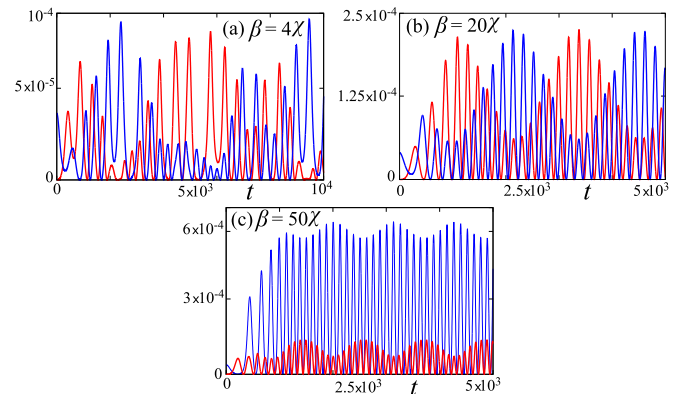

FIG. 11. Time evolution of the kinetic energies $P_1^2(t)$ (blue lines) and $P_2^2(t)$ (red lines) of the τ orbit for $\delta\mathcal{K} = 4\chi$ and (a) $\beta = 4\chi$, (b) $\beta = 20\chi$, and (c) $\beta = 50\chi$. The dipole-dipole interaction parameter is $\chi = 1 \times 10^{-5}$.

of the equipartition regime with the first dipole having most of the kinetic energy, the reference trajectory τ appears in the corresponding Poincaré maps inside a different type of KAM torus located at the periphery of the Poincaré map, as it is observed for $\beta = 50\chi$ and $\delta\mathcal{K} = 4\chi$ in Fig. 9(c), and for $\beta = 100\chi$ with $\delta\mathcal{K} = 4\chi$ and $\delta\mathcal{K} = 7\chi$ in Figs. 9(d) and 10(d), respectively. In these orbits, the kinetic energy $P_1^2(t)$ reaches significantly larger values than $P_2^2(t)$; see, for instance, $P_1^2(t)$ and $P_2^2(t)$ shown in Fig. 11(c) for $\delta\mathcal{K} = 4\chi$ and $\beta = 50\chi$. For other values of the excess energy $\delta\mathcal{K}$, not shown in Fig. 8, the second dipole could have most of the kinetic energy and the corresponding Poincaré surface of section of the trajectory τ is a KAM torus located around the central stable periodic orbit.

V. CONCLUSIONS

We have explored the classical phase space and related energy transfer mechanisms between two dipoles in the presence of a homogenous electric field. The dipoles are described by the rigid rotor approximation and are assumed to be fixed in space. In our numerical study, initially the dipoles are at rest in the stable lowest energy head-tail configuration. At $t = 0$, the system is pushed out of equilibrium by injecting a certain amount of kinetic energy to one of the dipoles. The following dynamics is investigated by analyzing in particular the kinetic energies of the dipoles and their time averages.

In the field-free case, and depending on the amount of excess energy in one of the dipoles, the system falls to either an energy equipartition regime or a nonequipartition one. The transition between these two regimes is abrupt and takes place at $\delta\mathcal{K} = 6\chi$. The analysis of the phase space structure of the system by means of Poincaré surfaces of section as well as a rotation of the Hamiltonian provide the explanation of this sharp transition.

The impact of the electric field on the energy transfer between the dipoles is quite dramatic. Depending on the field strength, the system shows different behaviors where equipartition, nonequipartition, and even chaotic regimes are possible. If the strengths of the dipole-dipole and electric field interactions are comparable, the energy transfer is a chaotic process and the time-averaged kinetic energies strongly depend on the field parameter and show rapid and sudden changes. Again, the phase space structure of the system by means of the Poincaré surfaces of section provides a global picture of the energy exchange mechanism.

We have here been focusing on an invariant subspace of the full dynamics and, therefore, it would be a natural continuation of this work to investigate the exchange of energy in the remaining part of the energy shell. Besides this, an extension of the system to a linear chain of dipoles is of immediate interest.

[1] *Photosynthetic Excitons*, edited by H. Van Amerongen, L. Valkunas, and R. Van Grondelle (World Scientific, Singapore, 2000).

[2] G. S. Engel, T. R. Calhoun, E. L. Read, T. K. Ahn, T. Mancal, Y. C. Cheng, R. E. Blankenship, and G. R. Fleming, Nature (London) **446**, 782 (2007).

[3] Y.-C. Cheng and G. R. Fleming, Annu. Rev. Phys. Chem. **60**, 241 (2009).

[4] J. l. Wu, F. Liu, J. Ma, R. J. Silbey, and J. Cao, J. Chem. Phys. **137**, 174111 (2012).

[5] *Energy Transfer Dynamics in Biomaterial Systems*, edited by I. Burghardt, V. May, D. A. Micha, and E. R. Bittner, (Springer-Verlag, Berlin, 2009).

[6] S. K. Saikin, A. Eisfeld, S. Valleau, and A. Aspuru-Guzik, Nanophotonics **2**, 21 (2013).

[7] D. Melnikau, D. Savateeva, V. Lesnyak, N. Gaponik, Y. Núñez Fernández, M. I. Vasilevskiy, M. F. Costa, K. E. Mochalov, V. Oleinikov, and Y. P. Rakovich, Nanoscale **5**, 9317 (2013).

[8] Y. Qiao, F. Polzer, H. Kirmse, E. Steeg, S. Kühn, S. Friede, S. Kirstein, and J. P. Rabe, ACS Nano **9**, 1552 (2015).

[9] A. S. Davydov, *Theory of Molecular Excitons* (McGraw-Hill, New York, 1962).

[10] R. Silbey, Annu. Rev. Phys. Chem. **27**, 203 (1976).

[11] J. D. Wright, *Molecular Crystals*, 2nd ed. (Cambridge University Press, Cambridge, U.K., 1994).

[12] *Cold Molecules: Theory, Experiments and Applications*, edited by R. Krems, B. Friedrich, and W. C. Stwalley (CRC Press, Boca Raton, FL, 2009).

[13] *Cold Atoms and Molecules*, edited by M. Weidemüller and C. Zimmermann (Wiley-VCH, Berlin, 2009).

[14] T. Lahaye, C. Menotti, L. Santos, M. Lewenstein, and T. Pfau, Rep. Prog. Phys. **72**, 126401 (2009).

[15] B. Zhu, J. Schachenmayer, M. Xu, F. H. Urbina, J. G. Restrepo, M. J. Holland, and A. M. Rey, New J. Phys. **17**, 083063 (2015).

[16] T. Sowiński, O. Dutta, P. Hauke, L. Tagliacozzo, and M. Lewenstein, Phys. Rev. Lett. **108**, 115301 (2012).

[17] M. Lemeshko, R. V. Krems, J. M. Doyle, and S. Kais, Mol. Phys. **111**, 1648 (2013).

[18] E. Fermi, J. Pasta, and S. Ulam, Los Alamos Report No. LA-1940, 1955 (unpublished).

[19] J. Ford, Phys. Rep. **213**, 271 (1992).

[20] G. P. Berman and F. M. Izrailev, Chaos **15**, 015104 (2005).
[21] T. Dauxois, M. Peyrard, and S. Ruffo, Eur. J. Phys. **26**, S3 (2005).
[22] *The Fermi-Pasta-Ulam Problem: A Status Report*, edited by G. Gallavotti (Springer-Verlag, Berlin, 2008).
[23] A. Mussot, A. Kudlinski, M. Droques, P. Szriftgiser, and N. Akhmediev, Phys. Rev. X **4**, 011054 (2014).
[24] D. Bambusi, A. Carati, A. Maiocchi, and A. Maspero, in *Hamiltonian Partial Differential Equations and Applications, Fields Institute Communications*, edited by P. Guyenne, D. Nicholls, and C. Sulem (Springer Science+Business Media, New York, 2015), p. 235.
[25] T. Penati and S. Flach, Chaos **17**, 023102 (2007).
[26] S. W. DeLeeuw, D. Solvaeson, M. A. Ratner, and J. Michl, J. Phys. Chem. B **102**, 3876 (1998).
[27] E. Sim, M. A. Ratner, and S. W. de Leeuw, J. Phys. Chem. B **103**, 8663 (1999).
[28] J. J. de Jonge, M. A. Ratner, S. W. de Leeuw, and R. O. Simonis, J. Phys. Chem. B **108**, 2666 (2004).
[29] R. J. Cross and R. G. Gordon, J. Chem. Phys. **45**, 3571 (1966).
[30] M. J. Norman, C. Chandre, T. Uzer, and P. Wang, Phys. Rev. A **91**, 023406 (2015).
[31] C. M. Dion, A. Keller, O. Atabek, and A. D. Bandrauk, Phys. Rev. A **59**, 1382 (1999).
[32] S. Trippel, T. Mullins, N. L. M. Müller, J. S. Kienitz, J. J. Omiste, H. Stapelfeldt, R. González-Férez, and J. Küpper, Phys. Rev. A **89**, 051401 (2014).
[33] E. Hairer, S. P. Norsett, and G. Wanner, *Solving Ordinary Differential Equations: I. Nonstiff Problems*, Springer Series in Computational Mathematics (Springer-Verlag, Berlin, 1993).